IFAC Journal of Systems and Control 35 (2026) 100379

Contents lists available at ScienceDirect

IFAC Journal of Systems and Control

journal homepage: www.elsevier.com/locate/ifacsc

Full Length Article

Reconstruction of Pressure Support Ventilation Signals: A Virtual Patient Set☆

K. Lindup [a], M. Bertoni [b], F. Padula [c,*], A. Visioli [d]

[a] School of Electrical Engineering, Computing, and Mathematical Sciences, Curtin University, Australia
[b] Department of Medical and Surgical Specialties, Radiological Science and Public Health, University of Brescia, Italy, and Spedali Civili di Brescia, Italy
[c] Curtin Centre for Optimisation and Decision Science, Curtin University, Australia
[d] Department of Mechanical and Industrial Engineering, University of Brescia, Italy

ARTICLE INFO

Article history:
Received 1 November 2025
Received in revised form 22 December 2025
Accepted 27 January 2026
Available online 4 February 2026

Keywords:
Mechanical ventilation
Assisted ventilation
Lung and diaphragm protective ventilation
Pressure support
Flow index
Mathematical modeling

ABSTRACT

Protection of the lungs and diaphragm is imperative to the safety of a patient receiving pressure support ventilation in the intensive care unit. To this end, accurate modeling of patient–ventilator interactions that occur within a breath is a vital step. Modeling of these interactions may be useful to better understand interactions that compromise patient safety, test in-silico new techniques to estimate physiological signals, and ultimately deliver safe ventilation. However, undisclosed and highly nonlinear internal ventilator dynamics hinder the derivation of such a model. Instead, in this paper, interactions were derived from clinical data, considering 400 breaths per patient to construct a set of 10 virtual patients. A simple first-order system was utilized to describe the interactions, with appropriate correlations between the system's gain and time constant, and the magnitude of the patient's effort to generalize the model. In parallel, generalized patient respiratory effort profiles were derived by analyzing similarities in measured efforts. Reconstruction of ventilator waveforms, utilizing the virtual patients, was achieved with a median accuracy greater than 85% in the worst case. A potential use case is also presented, further demonstrating the value of the presented virtual patients for in-silico development and validation of novel techniques. The derived virtual patients are shared via an online repository, and sufficient information is provided for readers to derive additional virtual patients.

1. Introduction

A clinical consensus exists that protection of a patient's lungs and diaphragm should be prioritized when providing assisted mechanical ventilation care, utilizing ventilation modes such as Pressure Support Ventilation (PSV) (Goligher, Dres et al., 2020). Concurrently, there is a desire to implement automation into aspects of ventilation (Morton et al., 2019). Combined, it is conceivable that closed-loop adjustment algorithms, that utilize breathing effort identification and monitoring techniques to promote lung and diaphragm protective ventilation (LDPV) (Goligher, Jonkman et al., 2020), will likely be developed in the near future. As outlined in Morton et al. (2019), when developing such an algorithm, models of the patient–ventilator interaction will be required to facilitate initial in-silico validation prior to clinical trials.

Recent literature related to PSV and LDPV has focused on identification and quantification of underlying patient breathing efforts (Kim et al., 2021; Reinders et al., 2022; Vicario et al., 2015). Whereas, development of models that describe Patient–Ventilator (P–V) interactions have been almost exclusively limited to control and proportional assist ventilation modes (Ang et al., 2022). Of those considering PSV, Crooke et al. (1998) present a general model of P–V interactions that occur within a breath, which, however, assumes perfect airway tracking of the target pressure support. In comparison, Zhang et al. (2021) propose a model that describes interactions that occur between breaths in response to changes in ventilator settings and sedative dosage. Of particular mention, Rees et al. (2022) present the "INVENT" Computerized Decision Support System (CDSS), which provides suggested changes to ventilator settings, as assessed by heuristic clinical preference models. The INVENT CDSS uses several models to capture breath-wise variation in patient-specific parameters that cannot be readily measured. However, this model focuses on patient contributions to minute ventilation rather than direct consideration of the pressures generated by patient respiratory effort.

A critical challenge yet to be addressed when developing a model that describes PSV specific within-breath P–V interactions is the relationship between ventilator-delivered airway flow (Q)

☆ This article is part of a Special issue entitled: 'IFAC WC 2026 - TC 8.2' published in IFAC Journal of Systems and Control.

* Corresponding author.
E-mail address: fabrizio.padula@curtin.edu.au (F. Padula).

https://doi.org/10.1016/j.ifacsc.2026.100379

Table 1
Patient characteristics and ventilator settings.

Pat.	Resistance R [$cmH_2O/L/s$]	Elastance E [cmH_2O/L]	Peak muscle pressure $\lvert P_{mus,\,peak}\rvert$ [cmH_2O]	Ventilator inspiration Time $t_{insp,\,vent}$ [s]	PEEP [cmH_2O]	PS_{upper} [cmH_2O]	Inspiratory rise Time T_{rise} [s]	Flow cycle [%]
1	10.9	15.1	7.90 (6.85, 9.07)	1.17 (1.08, 1.24)	6.0	11.0	0.15	0.3
2	20.1	13.2	11.7 (9.84, 13.7)	0.77 (0.73, 0.82)	8.0	14.0	0.10	0.3
3	26.7	41.0	20.6 (20.0, 21.5)	0.96 (0.94, 0.97)	9.5	16.5	0.15	0.3
4	15.0	15.5	10.0 (9.58, 10.4)	0.89 (0.80, 0.92)	12.0	22.0	0.15	0.3
5	14.5	21.4	6.52 (6.04, 7.12)	0.92 (0.90, 0.94)	10.0	20.0	0.15	0.3
6	10.2	23.6	8.57 (7.98, 9.17)	0.95 (0.88, 1.01)	9.0	14.0	0.15	0.3
7	12.0	16.5	10.4 (9.08, 11.9)	0.95 (0.89, 1.00)	8.0	14.0	0.05	0.3
8	9.53	30.4	17.3 (16.7, 17.9)	0.65 (0.63, 0.67)	8.0	16.0	0.15	0.3
9	13.8	20.2	7.76 (7.30, 8.32)	0.73 (0.69, 0.77)	10.0	18.0	0.15	0.3
10	13.9	14.6	12.7 (12.2, 13.0)	0.79 (0.76, 0.81)	11.0	23.0	0.10	0.3

$P_{mus,\,peak}$ and $t_{insp,\,vent}$ values presented as median (Inter Quartile Range). $P_{mus,\,peak}$ refers to peak negative pressure.

and pressure (P_{aw}). In general, it is acknowledged Q is supplied by the ventilator such that P_{aw} tracks a clinician set pressure support signal (PS). However, the internal ventilator feedback structure is not disclosed by ventilator manufacturers, and due to additional dynamics such as valves opening/closing, air leakages, and signal filtering, is also likely to be highly non-linear.

In this paper, a practical approach is proposed, where instead of developing a model based on first principles – which is extremely challenging given the complexity and gray-box nature of the system – a database of virtual patients was derived from clinical data. In particular, a multi-component model describing P–V interactions during PSV is presented for each patient, focusing on interactions that occur within a breath during the inspiration phase. Using readily available clinical data, each component of the model was derived via analysis of 400 consecutive breaths per patient. First, a general patient breathing effort waveform was constructed using basis spline (B-spline) curves, leveraging observed similarities between normalized measured breathing efforts. Second, interactions within the ventilator were modeled as a simple first-order system, with additional considerations for variation in the system dynamics in response to varying levels of respiratory effort.

A GitHub repository link has been included to allow for readers to interact with the virtual patient models directly. Further, the derivation of the patient models, as well as the general structure of the overall virtual patient model, has been described in detail to allow for readers with access to clinical data to expand upon the set of patients considered in this paper.

Excellent agreement – as quantified by $>$ 85% median similarity per patient for all patients – was observed between recorded and model-derived ventilator waveforms. Model value was further demonstrated through a potential use case, where changes in modeled flow signals, as captured by Flow Index (FI) measurements (Albani et al., 2021), were shown to realistically reflect corresponding changes in modeled respiratory efforts over a wide range of magnitudes. With the use of the model framework presented, a potential user could create realistic ventilator waveforms reflecting different patient types and levels of respiratory effort. These waveforms are especially valuable for in-silco validation of related control and estimation techniques, as existing models in literature do not realistically reflect the functionality of a PSV ventilator. The outcomes of this paper underpin the claim that the presented set of virtual patients can be conveniently used for testing of new control and estimation techniques, narrowing the gap between in-silico and in-vivo testing, and ultimately facilitating the development and adoption of novel techniques in assisted mechanical ventilation.

2. Patient data

Ten patients were considered in this study. These patients, aged 49-83, were a subset of a larger cohort of adult Acute Hypoxemic Respiratory Failure (AHRF) patients enrolled in the general Intensive Care Unit (ICU) at the University Hospital of Brescia, Italy. Ethical approval for the study protocol (Nº 6140) was obtained by the ethical review board in Brescia.

Patients were first ventilated under control ventilation modes before switching to PSV during weaning. All patients were invasively ventilated by a Servo-U 4.4.0 ventilator (Maquet Critical Care, Solna, Sweden), and ventilator signals were recorded by the Servo Tracker SCI, sampled at a rate of 100 Hz. Esophageal pressure (P_{es}) measurements were taken by nasogastric catheter (Sidam, Mirandola, Italy). 400 consecutive breaths were analyzed per patient to derive each virtual patient model. Breaths were selected for analysis proceeding occlusions used to confirm proper establishment of the esophageal catheter (Yoshida & Brochard, 2018). Utilizing the P_{es} signal, breaths were first visually analyzed to confirm the absence of patient–ventilator asynchronies. Relevant patient characteristics and ventilator settings are listed in Table 1.

3. Methods

The patient respiratory system was described by a single compartment lung model (Bates, 2009), where the negative pressure generated by the patient respiratory muscles was captured by the muscle pressure (P_{mus}). The model obeys the following equation:

$$P_{aw}(t) = Q(t)R + V(t)E + PEEP + P_{mus}(t), \tag{1}$$

where R and E are the resistance and elastance of the patient's respiratory system, respectively, PEEP (Positive End-Expiratory Pressure) is the target baseline pressure maintained during ventilator expiration, Q is the airway flow, and V is the tidal volume. To recreate breathing effort profiles, the underlying P_{mus} signal must be ascertained from the recorded ventilator signals. A gold standard estimate of P_{mus} can be obtained from esophageal pressure measurements ($P_{mus,\,es}$). However, $P_{mus,\,es}$ profiles are often distorted by cardio-genic and postural artifacts (Yoshida & Brochard, 2018). Instead, in this paper, P_{mus} was derived by inversion of the patient model (1). Nonetheless, information derived from the esophageal catheter has been used to ensure selected breaths are synchronous with the ventilator, and confirm that appropriate respiratory mechanics values and respiratory effort profiles were considered. See, for example, the agreement with $P_{mus,\,es}$ in Fig. 1.

3.1. Derive breathing profile from respiratory mechanics

An estimate of the P_{mus} signal can be derived by algebraic inversion of (1), a method first considered by Younes et al. (2007). Unlike other previous work that considers identification of underlying P_{mus} signals from data using least squares fitting (Sun

et al., 2024), here P_{mus} is reconstructed deterministically using measured signals and fixed respiratory mechanics parameters.

Given reliable estimates of patient respiratory mechanics [E_{est}, R_{est}], an estimate of P_{mus} ($P_{mus,\,rm}$) can be determined as

$$P_{mus,\,rm}(t) = P_{aw}(t) - \left[Q(t)R_{est} + V(t)E_{est} + PEEP\right]. \tag{2}$$

Respiratory mechanics for the derived virtual patients are presented in Table 1. Respiratory mechanics were estimated by Least Squares Fitting (LSF) during the initial control ventilation period in the absence of respiratory effort (Rossi et al., 1985). End-inspiratory occlusions close to the recorded 400 breaths were used during PSV to confirm the validity of the estimated E (Younes et al., 2001). The validity of R was confirmed by the absence of a plateau in the identified patient effort (Pasillas-Lépine et al., 2024). Finally, respiratory mechanics estimates obtained by LSF utilizing $P_{mus,\,es}$, as described in Vicario et al. (2015), were also considered to confirm the estimated values. Of note, this final consideration is not required for the derivation of a virtual patient where P_{es} recordings are not available.

The above protocol yields a breathing profile for a single breath. To provide a general solution, such that ventilator waveforms in response to respiratory efforts of arbitrary magnitude and duration can be generated, a framework was proposed to derive a general breathing model for a given patient.

3.2. B-spline general model

For each patient, a generalized breathing profile ($\hat{P}_{mus}$) was derived from analysis of 400 consecutive breaths. The breathing profile was determined from $P_{mus,\,rm}$ under the assumption that the typical profile does not vary significantly over short periods of time. More specifically, it was assumed that minimal variation in $P_{mus,\,rm}$ should be observed where profiles are normalized relative to the peak measured negative pressure per breath ($P_{mus,\,peak}$) and time-scaled such that all considered inspiratory pressure profiles are of equal duration.

For each breath, a $P_{mus,\,rm}$ signal was derived by (2), using respiratory mechanics values listed in Table 1. Referring to Fig. 1, $P_{mus,\,rm}$ was defined from the observed onset of respiratory effort (t_{trig}) to the onset of the subsequent respiratory effort. $P_{mus,\,rm}$ was first time-scaled ($P_{mus,\,n}$) such that the patient inspiration phase ($T_{insp,\,pat}$) of each breath was equal to $T_{nom} = 150$ samples (1.5 s). Here, $T_{insp,\,pat}$ was defined from $t = t_{onset}$ to the point of ventilator cycling off (t_{cycle}), as shown in Fig. 1. Then, $P_{mus,\,n}$ was normalized and it was assumed that $P_{mus,\,rm} \leq 0$ [cmH_2O] during both inspiration and expiration, so that

$$\tilde{P}_{mus,\,n} = \max\left(0,\ \frac{P_{mus,\,n}}{P_{mus,\,peak}}\right). \tag{3}$$

Finally, B-spline functions were used to characterize and reconstruct $\tilde{P}_{mus,\,n}$, and subsequently construct a unique modeled breathing profile ($\hat{P}_{mus}$) per patient.

B-spline curves have previously been used to describe breathing efforts (Knopp et al., 2021; Lindup et al., 2024). The use of splines facilitates a relatively small set of model variables, whilst providing greater flexibility to the shape of the breathing profile as compared to existing models (Knopp et al., 2024). The $\tilde{P}_{mus,\,n}$ signal profile was reconstructed by considering the linear combination of M second order ($d = 2$) B-splines ($\phi_{2,j}$) scaled by a corresponding set of spline coefficients ($P_{s,j}$). This reconstruction of the breathing profile yields:

$$\tilde{P}_{mus,\,n} \approxeq \hat{P}_{mus}(t) = \sum_{j=1}^{M} -P_{s,j}\phi_{2,j}(t), \tag{4}$$

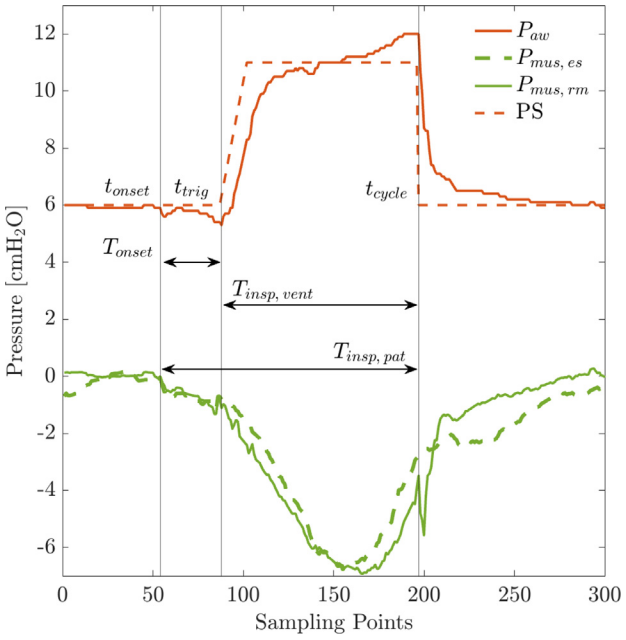

Fig. 1. Example of target pressure support (PS), measured airway pressure (P_{aw}), and derived muscle pressure waveform estimates from P_{es} measurements ($P_{mus,\,es}$) and estimated respiratory mechanics ($P_{mus,\,rm}$).

where B-spline ($\phi_{2,j}$) curves are defined recursively as

$$\phi_{0,j}(t) = \begin{cases} 1, & T_j < t < T_j + 1 \\ 0, & \text{otherwise,} \end{cases}$$

$$\phi_{d,j}(t) = \frac{t - T_j}{T_{j+d} - T_j}\phi_{d-1,j}(t) + \frac{T_{j+d+1} - t}{T_{j+d+1} - T_{j+1}}\phi_{d-1,j+1}(t),\ d \geq 1, \tag{5}$$

where T_j are equally spaced points in time with spacing between points equal to the knot width ($k_w = 0.25$). Selection of k_w was determined by a sensitivity analysis, presented in the Supplementary Material.

An $M \times N$ matrix ($\boldsymbol{B}$) containing $\phi_{2,j}$ curves described at each sampled point in time (t_i) was fit to individual $\tilde{P}_{mus,\,n}$ profiles. This fitting obtained a set of spline coefficients ($\overrightarrow{P_s}$), which was then used to describe $P_{mus,\,spline}$ as per (4). To ensure that the same nominal B-spline matrix could be considered for all breaths with varying lengths, $N = 700$ data points (i.e., 7 s sampled at 100 Hz) were used to ensure that the number of columns of $\boldsymbol{B}$ exceeded the number of samples of each individual respiratory effort. The corresponding number of B-spline functions was $M = N/k_w + d = 30$. The B-spline coefficients were then obtained by solving $\boldsymbol{B}^\top\boldsymbol{B}\overrightarrow{P_s} = \boldsymbol{B}^\top\overrightarrow{y}$, where

$$\boldsymbol{B} = \begin{bmatrix} \phi_{2,1}(t_1) & \phi_{2,1}(t_2) & \dots & \phi_{2,1}(t_N) \\ \phi_{2,2}(t_1) & \ddots & & \vdots \\ \vdots & & \ddots & \vdots \\ \phi_{2,M}(t_1) & \phi_{2,M}(t_2) & \dots & \phi_{2,M}(t_N) \end{bmatrix},\ \overrightarrow{P_s} = \begin{bmatrix} P_{s,1} \\ P_{s,2} \\ \vdots \\ P_{s,M} \end{bmatrix},$$

$\overrightarrow{y} = [\tilde{P}_{mus,\,n},\ \overrightarrow{0}\,]^\top$ and $\overrightarrow{0}$ is a vector of zeros of appropriate dimension. Fig. 2 illustrates the IQR distribution of $P_{s,j}$ values for each B-spline determined from the described fitting protocol, considering Patient 1. Similar results for all patients, as well as median $P_{s,j}$ values used to construct $\hat{P}_{mus}$ for each patient via (4), profiles are presented in the Supplementary Material.

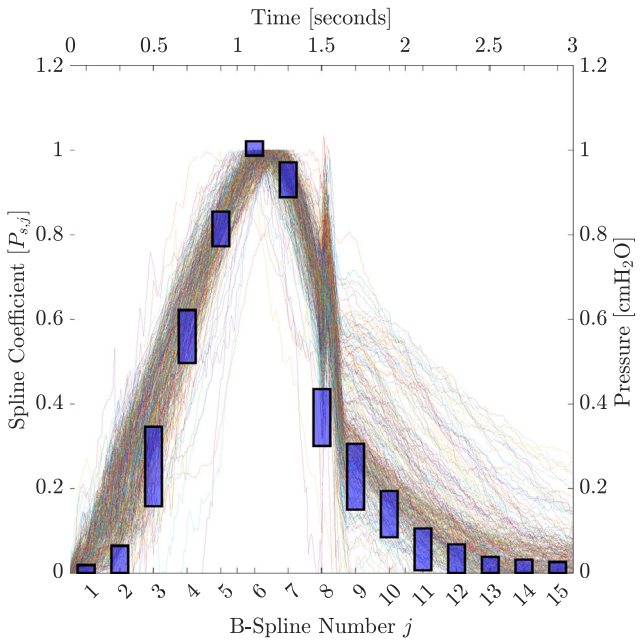

Fig. 2. Patient 1 B-spline coefficient IQR distributions determined from 400 normalized breathing efforts.

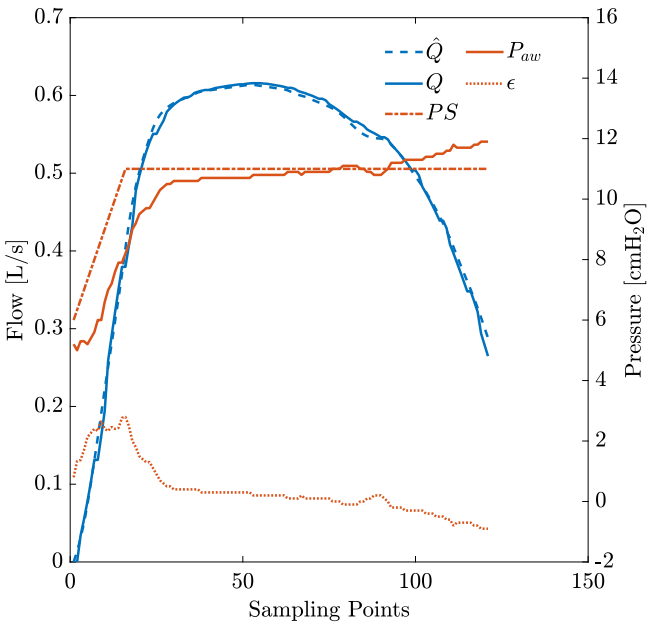

Fig. 3. xample modeled flow signal ($\hat{Q}$), derived from error (ϵ) between airway pressure (P_{aw}) and pressure support target (PS), versus measured flow signal (Q).

Last, $\hat{P}_{mus}$ was normalized as in (3) to ensure peak $\hat{P}_{mus} = 1$ [cmH$_2O$]. To generate any desired respiratory effort, $\hat{P}_{mus}$ could then be readily scaled by some value $P_{mus,\,peak}$, and resampled in time to a desired duration.

3.3. Ventilator model

Considering PSV, ventilator support is initiated by the patient's breathing efforts. Ventilators are most often either pressure- or flow-triggered (Hess, 2005), and cycle off when Q falls below some percentage ($\%Q_{cycle}$) of the observed peak flow. At the point of triggering, a time-varying pressure support (PS) target increases linearly from PEEP to some absolute upper value during inspiration (PS_{upper}). This increase occurs over a defined inspiratory rise time (T_{rise}), such that the rate of increase is defined by $m = (PS_{upper} - PEEP)/T_{rise}$. PS then remains equal to PS_{upper} until ventilator cycling. For a given breath where triggering (t_{trig}) occurs at t = 0, PS can be described as follows

$$PS(t) = \begin{cases} m \cdot t + PEEP & \text{for } t_{trig} \le t \le t_{trig} + t_{rise}, \\ PS_{upper} & \text{for } t > t_{trig} + t_{rise}. \end{cases} \tag{6}$$

It is commonly assumed that, during PSV, the ventilator is a flow generator that regulates the flow as a function of the error (ϵ) between the target and measured airway pressure signals. This relationship can, however, be highly complicated due to multiple factors, including nonlinear dynamics (e.g., the inspiratory valve), unmodeled dynamics (e.g., leaks and air compressibility), and undisclosed ventilator control and filtering algorithms. For example, a standard proportional–integral–derivative controller, considering the airway pressure error as the input, is clearly unable to produce the flow signal in Fig. 3.

In this paper, a gray-box solution was proposed in which clinical data was fit to an assumed simple relationship between Q and P_{aw}. Utilizing a simple first-order system (C), Q can be accurately reconstructed by passing the error between PS and P_{aw}, $\epsilon(t) = PS(t) - P_{aw}(t)$, through C to generate a modeled flow signal ($\hat{Q}$).

In the Laplace domain, $C(s)$ is defined as

$$C(s) = \frac{K}{\tau s + 1}, \tag{7}$$

characterized by its DC-gain K and time constant τ. Therefore, $\hat{Q}(s) = C(s)\epsilon(s) = \frac{K}{\tau s+1}(PS(s) - P_{aw}(s))$. The structure of $C(s)$ was selected to ensure accurate $\hat{Q}$ profiles whilst avoiding over-parameterization.

Aligning with the protocol described in Section 3.2, for each patient, model fitting was performed per breath for 400 consecutive breaths. A unique $\hat{Q}$ profile was generated for each breath by selection of $[K, \tau]$ on a per breath basis via least squares minimization of $Q(t) - Q(t_{trig}) - \hat{Q}(t)$, where the constant term $Q(t_{trig})$ overcomes the limitation due to the fact that $\hat{Q}$ obtained using $C(s)$ cannot account for the observed non-zero flow generated by the patient during the onset of effort, prior to ventilator triggering.

Model fitting was performed over ventilator inspiration ($T_{insp,\,vent}$), defined as t_{trig} to t_{cycle} (see Fig. 1). An example fitting for Patient 1 is provided in Fig. 3. It was observed that, while $\hat{Q}$ overlapped Q with minimal difference, K and τ values varied between fittings. As such, to provide a general patient–ventilator model for an arbitrary P_{mus} input, relationships between $P_{mus,\,peak}$ and ventilator parameters were analyzed on a per patient basis (see Table 2). For a given patient, where relationships between $P_{mus,peak}$ and K, and between K and τ were statistically significant (two-tailed p-test < 0.05), these relationships were implemented into the relevant virtual patient model. In comparison, if not statistically significant, median respective K and/or τ values were considered instead. Where statistically significant, R^2 values determined from K and $P_{mus,\,peak}$ relationships varied from 0.04 – 0.49. Further, for all patients, statistically significant relationships between $t_{insp,\,vent}$ and $P_{mus,\,peak}$ were identified. Moderate to strong correlations between K and τ were also observed (R^2 = 0.20-95 for all except Patient 4).

Table 2
Identified patient–ventilator interaction model parameters and relationships.

Pat.	K	τ	K vs $P_{mus,\,peak}$				$t_{insp,\,vent}$ vs $P_{mus,\,peak}$				K vs τ			
			m	y-int	R^2	*p-value*	m	y-int	R^2	*p-value*	m	y-int	R^2	*p-value*
1	2650 (2560, 2740)	1.79 (1.73, 1.83)	48.8	1990	0.49	✓	4.67	79.1	0.54	✓	5.00E−04	0.68	0.40	✓
2	1780 (1720, 1860)	1.43 (1.37, 1.49)	−26	2100	0.21	✓	1.61	61.2	0.92	✓	4.00E−04	0.781	0.21	✓
3	4330 (3420, 5370)	2.90 (2.58, 3.31)	−61.7	5730	0.01	0.13	1.13	78.8	0.18	✓	4.43E−04	0.998	0.95	✓
4	987 (959, 1010)	0.779 (0.756, 0.806)	−9.58	1085	0.04	✓	1.12	70.631	0.09	✓	7.39E−05	0.705	0.01	0.07
5	1700 (1630, 1830)	1.41 (1.37, 1.46)	12.1	1670	0.01	0.18	1.96	79.3	0.21	✓	3.03E−04	0.89	0.63	✓
6	1700 (1620, 1800)	1.21 (1.17, 1.26)	−51.8	2170	0.09	✓	4.40	56.7	0.33	✓	4.71E−04	0.406	0.76	✓
7	1380 (1320, 1430)	1.14 (1.03, 1.23)	−24.7	1640	0.46	✓	1.87	74.6	0.18	✓	1.37E−03	−0.758	0.76	✓
8	926 (899, 959)	0.651 (0.605, 0.703)	−23.7	1340	0.19	✓	1.87	32.8	0.45	✓	8.52E−04	−0.141	0.70	✓
9	1360 (1310, 1420)	1.04 (1.00, 1.07)	−67.2	1890	0.39	✓	−2.86	95	0.27	✓	5.92E−04	0.211	0.49	✓
10	401 (395, 406)	0.316 (0.298, 0.329)	−5.75	472	0.10	✓	−2.57	111	0.14	✓	1.70E−03	−0.367	0.46	✓

K and τ values presented as median (IQR). ✓denotes statistically significant relationships ($p-$value < 0.05.)

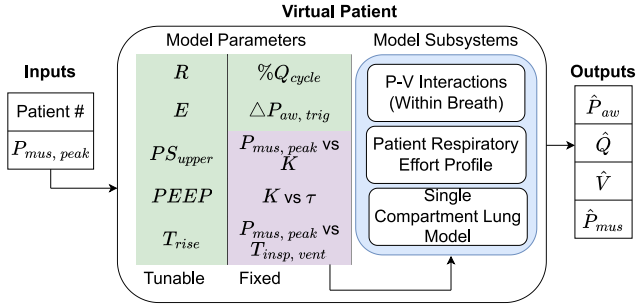

Fig. 4. Virtual patient model framework.

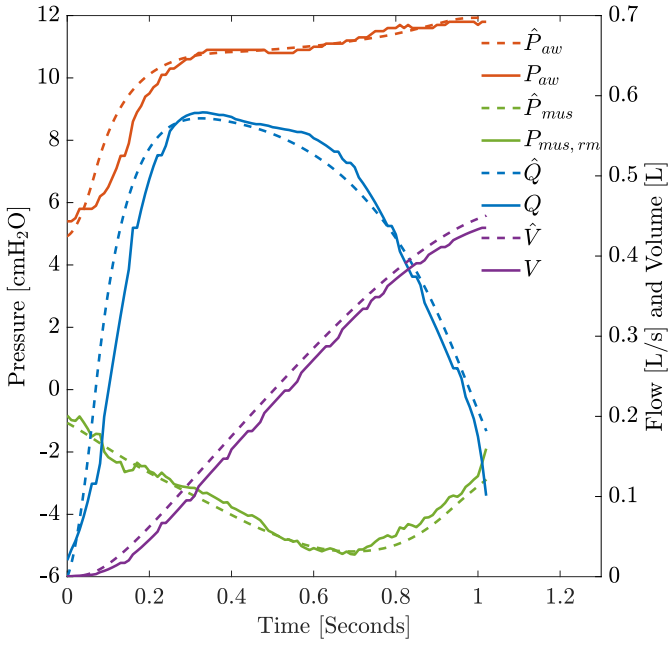

Fig. 5. Example of inspiratory measured ventilator waveforms, including airway pressure (P_{aw}), flow (Q) and volume (V) and estimated muscle pressure ($P_{mus,rm}$) compared to their modeled ($\hat{\cdot}$) equivalent signals.

4. Virtual patients assessment

In this section, the ability of derived virtual patient models to recreate realistic clinical physiological signals will be assessed against signals logged by the Servo-U ventilator. Further, an explanation of how to use the virtual patient models provided will be outlined, and an example use case will be presented to demonstrate the ability of the model to generate realistic signals for a wide range of peak muscle pressure magnitudes.

The performance of the model was first evaluated by reconstructing the ventilator signals of the 400 breaths considered, constraining the model ventilator inspiratory time to align with the recorded $T_{insp,\,vent}$. For each breath, $\hat{P}_{mus}$ was scaled by the corresponding measured $P_{mus,\,peak}$ and time-scaled by the ratio between $T_{insp,pat}$ and T_{nom}. To evaluate the model's ability to accurately recreate recorded ventilator signals, signal agreement was quantified by: (i) the difference between model and recorded peak values, (ii) the Integral Absolute Error (IAE) between the modeled and recorded signals, and (iii) the percentage IAE as the ratio of the IAE and the area under the measured curve (%IAE).

Fig. 5 compares modeled and measured ventilator signals of a single inspiration phase, considering Patient 1. Table 3 contains the results from the first scenario, where $\epsilon(\cdot)$ denotes the difference between measured and modeled signals, and $IAE_{\epsilon(\cdot)}$ and $\%IAE_{\epsilon(\cdot)}$ denote the IAE and its percentage variation for the specific signal detailed in the subscript. Overall, the agreement across all patients and considered signals exceeded a median accuracy of 85%, highlighting the ability of the model to accurately describe the P–V interactions within a breath. Similar results for $P_{mus,\,rm}$ are included in the Supplementary Material.

Fig. 4 illustrates the overall structure of the virtual patient model. First, a user can select a desired virtual patient (*i.e.,* patient number corresponding to each patient listed in Table 1) and desired peak respiratory effort. As listed in Table 2, correlations between $P_{mus,\,peak}$ and $T_{insp,\,vent}$ have been identified, such that for a selected peak respiratory effort, the duration of the effort is scaled appropriately. The model, using stored respiratory mechanics values, ventilator settings, and derived P–V interaction model parameters, will then produce a $\hat{P}_{mus}$ signal and corresponding modeled ventilator waveforms. Further, a user can also then adjust patient respiratory mechanics and ventilator settings to consider more general scenarios, and for example, perform Monte Carlo testing. Source code is available at: https://github.com/kaelancl/Virtual-Patient-PSV

An example use-case of the virtual patient model is also presented, considering Patient 1. For other patients, results have been omitted here for brevity and are instead included in the Supplementary Material. In this example, a pressure-triggered ventilator was modeled where $\triangle P_{aw} = 1$ [cmH$_2$O] below PEEP is sufficient to trigger the ventilator ($\triangle P_{aw,\,trig}$), and $\%Q_{cycle} = 30\%$. $P_{mus,\,peak}$ was incrementally increased from 1 cmH$_2$O to the maximum observed $P_{mus,\,peak}$ for a given patient over 100 modeled breaths. Where statistically significant relationships were observed as listed in Table 2, $t_{insp,\,vent}$ was scaled by $P_{mus,\,peak}$ and subsequently, in addition with the median observed T_{onset}, was used to time-scale $\hat{P}_{mus}$. Flow Index (FI) values, first described in Albani et al. (2021), were determined on a per breath basis to track changes in the curvature of inspiratory $\hat{Q}$ profiles in response to changes in the peak magnitude of $\hat{P}_{mus}$. As means of comparison, FI values were also determined per breath considering the 400 Q profiles used to derive the virtual patient model. In

Table 3
Reconstruction of ventilator waveforms using derived virtual patients.

Pat.	Q_{peak} [mL/s]	V_{peak} [L]	$P_{aw,\,peak}$ [cmH$_2$O]	$\epsilon(Q_{peak})$ [mL/s]	$\epsilon(V_{peak})$ [L]	$\epsilon(P_{aw,\,peak})$ [cmH$_2$O]
1	635 (610, 671)	605 (539, 667)	12.0 (11.8, 12.1)	17.9 (−28.6, 52.8)	0.517 (−7.85, 9.99)	−0.022 (−0.171, 0.112)
2	686 (646, 738)	424 (387, 477)	15.4 (15.0, 15.6)	−49.3 (−80.6, −20.1)	−47.6 (−57.7, −36.4)	−0.313 (−0.472, −0.179)
3	633 (621, 642)	479 (470, 489)	17.7 (17.6, 17.9)	4.22 (−27.1, 24.3)	6.29 (−5.86, 21.1)	−0.153 (−0.362, 0.040)
4	944 (932, 955)	587 (568, 608)	23.2 (23.1, 23.3)	51.4 (34.5, 66.5)	−34.9 (−42.6, −27.3)	0.119 (0.028, 0.211)
5	801 (793, 818)	508 (490, 529)	20.9 (20.8, 21.0)	76.8 (66.0, 88.2	0.51 (−3.27, 3.39)	−0.070 (−0.15, 0.008)
6	694 (666, 718)	475 (453, 495)	14.6 (14.5, 14.7)	−15.8 (−52.9, 9.43)	−7.76 (−18.2, 1.64)	−0.117 (−0.203, 0.014)
7	721 (686, 775)	598 (550, 652)	15.6 (15.6, 15.8)	−9.12 (−27.8, 12.4)	−25.4 (−36.6, −14.9)	−0.673 (−0.904, −0.477)
8	1170 (1150, 1190)	624 (605, 647)	18.2 (18.1, 18.2)	55.8 (39.8, 67.9)	−8.52 (−14.7, −3.39)	−0.759 (−0.855, −0.661)
9	726 (712, 750)	418 (401, 435)	19.1 (19.0, 19.2)	−38.2 (−54.2, −21.5)	−40.5 (−47.0, −34.0)	0.047 (−0.008, 0.126)
10	1090 (1080, 1100)	717 (697, 735)	23.9 (23.8, 24.0)	−76.2 (−87.1, −63.9)	−65.2 (−74.0, −55.9)	0.073 (0.016, 0.144)
	$IAE_{\epsilon(P_{aw})}$	$IAE_{\epsilon(Q)}$	$IAE_{\epsilon(V)}$	$\%IAE_{\epsilon(P_{aw})}$	$\%IAE_{\epsilon(Q)}$	$\%IAE_{\epsilon(V)}$
1	0.372 (0.308, 0.454)	57.4 (38.1, 85.6)	21.8 (11.6, 37.5)	3.15 (3.12, 3.16)	12.6 (12.3, 12.8)	8.93 (8.35, 9.47)
2	0.351 (0.310, 0.415)	51.3 (42.1, 62.8)	23.9 (18.8, 29.4)	3.34 (3.27, 3.39)	12.0 (11.4, 12.4)	12.1 (11.7, 13.1)
3	0.556 (0.472, 0.643)	54.5 (36.9, 78.1)	23.6 (12.3, 32.6)	3.50 (3.48, 3.51)	12.3 (11.9, 12.4)	9.44 (9.32, 9.48)
4	0.673 (0.631, 0.717)	60.4 (55.8, 65.7)	16.3 (12.1, 20.2)	3.71 (3.6, 3.74)	10.1 (9.91, 10.5)	6.31 (6.17, 6.43)
5	0.562 (0.511, 0.607)	54.3 (49.4, 58.9)	7.61 (6.85, 8.72)	3.26 (3.24, 3.26)	10.5 (10.2, 10.5)	3.42 (3.39, 3.47)
6	0.360 (0.322, 0.409)	38.9 (30.3, 49.3)	11.4 (6.71, 21.1)	2.76 (2.72, 2.78)	8.61 (8.37, 9.46)	5.98 (5.81, 6.65)
7	0.222 (0.196, 0.252)	34.7 (28.2, 43.8)	15.0 (7.61, 23.3)	1.76 (1.75, 1.78)	6.42 (6.36, 6.55)	6.20 (5.58, 6.38)
8	0.413 (0.372, 0.448)	46.3 (40.8, 52.3)	7.90 (5.52, 11.4)	4.22 (4.21, 4.24)	7.73 (7.63, 7.81)	4.86 (4.74, 5.47)
9	0.427 (0.403, 0.453)	46.7 (41.9, 51.5)	22.9 (20.2, 25.9)	3.38 (3.28, 3.77)	11.8 (11.5, 12.8)	14.1 (14.0, 14.2)
10	0.419 (0.392, 0.459)	68.8 (60.3, 76.7)	34.1 (30.1, 37.5)	2.54 (2.53, 2.6)	10.2 (9.92, 10.4)	11.5 (11.3, 11.6)

Results presented as median (IQR).

this way, comparing model and data derived *FI* values provides an indication of the model's ability to recreate realistic waveforms over a wide range of respiratory efforts. Two trend-lines, with the *y*-intercepts forced through the origin (0,0), were identified between model-derived ($\hat{FI}$) and data-derived *FI* values, versus respective modeled and measured $P_{mus,\,peak}$ values.

Fig. 6 illustrates the considered example, highlighting observed overlap between $\hat{FI}$ and measured *FI* values. The distribution of measured *FI* values was shown by boxplots, categorized by $P_{mus,\,peak}$ absolute value: small ($|P_{mus,\,peak}| \leq 5$ cmH$_2$O), moderate (5 cmH$_2$O $< |P_{mus,\,peak}| <$ 10 cmH$_2$O), and large ($|P_{mus,\,peak}| \geq$ 10 cmH$_2$O) efforts, aligning with clinical classifications (Goligher, Dres et al., 2020). In comparison, $\hat{FI}$ versus model $|P_{mus,\,peak}|$ value pairs were illustrated by the blue circle data points (modeled $|P_{mus,\,peak}|$ axis labels not shown for clarity). Statistically significant relationships were observed between respective $P_{mus,\,peak}$, and both measured *FI* and $\hat{FI}$. For Patient 1, very similar trend line gradient (m) values for $\hat{FI}$ (m = 0.589) and *FI* (m = 0.590) were observed, demonstrating that the model was able to capture changes in respiratory effort by appropriate changes in the Q profile. Similar trends can be observed for the other patients in the Supplementary Material.

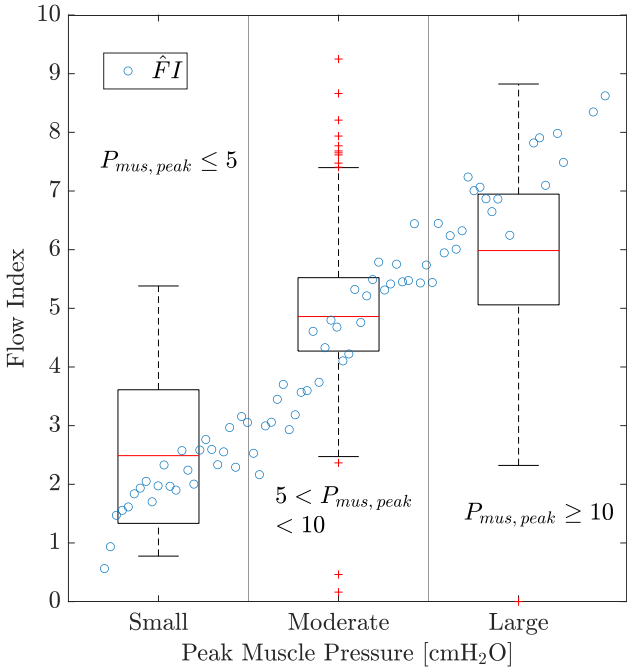

Fig. 6. Modeled (blue circle) and measured (boxplots) Flow Index (*FI*) values versus peak muscle pressure ($|P_{mus,\,peak}|$), considering modeled and measured respiratory efforts respectively. Results for Patient 1.

5. Discussion

In this paper, a database of modeled P–V within-breath interactions is presented, generated from clinical data across 10 patients and 400 breaths per patient. Modeled ventilator signals of P_{aw}, Q, and V, reflected their measured counterparts with minimal error. The accuracy of the modeled ventilator signals was dependent on two main factors: i) the variance of $P_{s,j}$ per B-spline between breaths, and (ii) the proportion of variance of K and τ that could be explained by $P_{mus,\,peak}$.

Determined $P_{s,j}$ values for each patient are shown in the Supplementary Material. First, considering Patient 1 as an example, generally tight $P_{s,j}$ distributions were observed. The least $P_{s,j}$ variation was observed at B-spline $j = 6$ (1.007 [0.987, 1.021]), while the greatest variation was observed at B-spline $j = 3$ (0.267 [0.158, 0.346]). Minimal variation in $P_{s,j}$ for B-spline $j = 3$ implies that the point of peak effort relative to the duration of $T_{insp,\,pat}$ varies minimally. By comparison, considering Patient 2, median $P_{s,j}$ values for B-splines j = [4,5,6] are all > 0.9. As such, for this patient, greater variability in the location of peak effort relative to $T_{insp,\,vent}$ was observed. Furthermore, greater variation in $P_{s,j}$ at B-spline $j = 3$ can be generally expected, given the steepness of $\hat{P}_{mus,n}$ around that point within the breath. As such, these results highlight the relative degree of intra-patient variability per patient, and thus, the extent to which $\hat{P}_{mus}$ profiles are representative of the total sets of breaths analyzed. In comparison, variation in median $P_{s,j}$ and therefore, $\hat{P}_{mus}$ between patients signifies significant inter-patient variability. This outcome highlights the strength of the considered derivation approach in its ability to adjust the modeled breathing profile to accommodate for these variations.

Second, as introduced as part of the motivation for this study, the relationship between ventilator delivered Q and P_{aw} is likely

to be impacted by a number of unmeasured factors, including valve dynamics and air leakages. As illustrated by Fig. 3, $\hat{Q}$ derived as in Section 3.3, accurately reflected the Q profile. Though, as listed in Table 2, derived $[K, \tau]$ values were subject to large inter-patient variability and small intra-patient variability. The latter is likely linked to variations in respiratory effort as highlighted by the correlations listed in Table 2. Where statistically significant, the proportion of variance that could be explained by these correlations ranged from 4−95%, suggesting that degree to which the ventilator model can be generalized for an arbitrary effort is highly patient specific. In any case, comparing *%IAE* results listed in Table 2 between patients, any unexplained variation in $[K, \tau]$ did not prevent the model from reproducing the considered P–V interactions with sufficient accuracy to replicate the considered scenarios. As such, these results provide further justification for the rationale that the model should be simple enough that it is easily reproducible yet complex enough to accurately recreate the observed P–V interactions.

6. Conclusions

In this paper, a set of virtual patient models was presented that describe the interactions between the patient and ventilator within a breath during PSV. The devised intra-breath patient models were derived from clinical data, considering 400 consecutive breaths per patient. Excellent agreement between the modeled and measured ventilator signal profiles was achieved, as evaluated by the percentage integral absolute error between modeled and measured signals ($<$ 15% median *%IAE* in all cases). A potential use case of these models was also presented, demonstrating how each model captures changes in P–V interactions over a wide range of respiratory effort magnitudes. These outcomes provide strong evidence that the virtual patient model framework could provide a tool for in-silico development and validation of patient monitoring techniques and closed loop solutions to titrate LDPV.

The proposed model framework was intended to be generalizable in its methodology, rather than through reuse of previously derived models for a new patient. Though the presented virtual patient set were derived from a single adult AHRF cohort, ventilated using a Servo-U ventilator, new virtual patient models can be derived from routinely available ventilator signals following the presented methodology.

Of note, the study focused on the analysis of synchronous breathing efforts. At times in ICU, ventilator support may not align with the timing of the patient's efforts, leading to patient–ventilator asynchrony. Considering a clinical implementation of a virtual patient, an asynchrony detection algorithm, such as those presented in Rietveld et al. (2025), would be utilized alongside to identify and discard asynchronous breaths. Further evaluation of the accuracy of the virtual patient models when considering asynchronous P–V interactions could also further enhance the model framework's clinical and research value. Though not the focus of this paper, validation of the model framework against a dedicated validation dataset could be undertaken to evaluate its potential use to predict ventilator signal profiles for prior unseen clinical scenarios. Finally, the development of an inter-breath model that quantifies the expected variation of the magnitude of the patient's effort in response to changes in ventilator settings would complement the proposed intra-breath model, yielding a realistic set of patient digital twins.

CRediT authorship contribution statement

K. Lindup: Writing – original draft, Software, Methodology, Investigation, Data curation, Conceptualization. **M. Bertoni:** Resources. **F. Padula:** Writing – review & editing, Supervision, Methodology, Conceptualization. **A. Visioli:** Writing – review & editing, Supervision.

Declaration of competing interest

The authors declare that they have no known competing financial interests or personal relationships that could have appeared to influence the work reported in this paper.

Appendix A. Supplementary data

Supplementary material related to this article can be found online at https://doi.org/10.1016/j.ifacsc.2026.100379.

Data availability

The data that have been used is confidential.

References

Albani, F., Pisani, L., Ciabatti, G., Fusina, F., Buizza, B., Granato, A., Lippolis, V., Aniballi, E., Murgolo, F., Rosano, A., et al. (2021). Flow index: a novel, non-invasive, continuous, quantitative method to evaluate patient inspiratory effort during pressure support ventilation. *Critical Care*, *25*(1), 1–11.

Ang, C., Lee, J., Chiew, Y., Wang, X., Tan, C., Cove, M., Nor, M., Zhou, C., Desaive, T., & Chase, G. (2022). Virtual patient framework for the testing of mechanical ventilation airway pressure and flow settings protocol. *Computer Methods and Programs in Biomedicine*, *226*, Article 107146.

Bates, J. H. (2009). *Lung mechanics: an inverse modeling approach*. Cambridge University Press.

Crooke, P., Head, J., Marini, J., & Hotchkiss, J. (1998). Patient–ventilator interaction: A general model for nonpassive mechanical ventilation. *Mathematical Medicine and Biology: A Journal of the IMA*, *15*(4), 321–337.

Goligher, E., Dres, M., Patel, B., Sahetya, S., Beitler, J., Telias, I., Yoshida, T., Vaporidi, K., Grieco, D., Schepens, T., et al. (2020). Lung and diaphragm-protective ventilation. *American Journal of Respiratory and Critical Care Medicine*, *202*(7), 950–961.

Goligher, E., Jonkman, A., Dianti, J., Vaporidi, K., Beitler, J., Patel, B., Yoshida, T., Jaber, S., Dres, M., Mauri, T., et al. (2020). Clinical strategies for implementing lung and diaphragm-protective ventilation: avoiding insufficient and excessive effort. *Intensive Care Medicine*, *46*(12), 2314–2326.

Hess, D. (2005). Ventilator waveforms and the physiology of pressure support ventilation. *Respiratory Care*, *50*(2), 166–186.

Kim, K. T., Knopp, J., & Chase, J. G. (2021). Quantifying patient spontaneous breathing effort using model-based methods. *Biomedical Signal Processing and Control*, *69*, Article 102809.

Knopp, J., Chase, G., Kim, K., & Shaw, G. (2021). Model-based estimation of negative inspiratory driving pressure in patients receiving invasive NAVA mechanical ventilation. *Computer Methods and Programs in Biomedicine*, *208*, Article 106300.

Knopp, J., Chiew, Y., Georgopoulos, D., Shaw, G., & Chase, G. (2024). Ubiquity of models describing inspiratory effort dynamics in patients on pressure support ventilation. *IFAC Journal of Systems and Control*, *27*, Article 100250.

Lindup, K., Chase, J., Zhou, C., Bertoni, M., Padula, F., & Visioli, A. (2024). Non-invasive patient breathing effort identification: a b-spline and mixed integer solution. *IFAC-PapersOnLine*, *58*(24), 187–192.

Morton, S., Knopp, J., Chase, G., Docherty, P., Howe, S., Möller, K., Shaw, G., & Tawhai, M. (2019). Optimising mechanical ventilation through model-based methods and automation. *Annual Reviews in Control*, *48*, 369–382.

Pasillas-Lépine, W., Tuffet, S., Soussen, C., Gendreau, S., Boujelben, M., Mekontso-Dessap, A., & Carteaux, G. (2024). A novel method for noninvasive estimation of respiratory effort during pressure support ventilation. *Biomedical Signal Processing and Control*, *93*, Article 106176.

Rees, S., Spadaro, S., Corte, F. D., Dey, N., Brohus, J., Scaramuzzo, G., Lodahl, D., Winding, R., Volta, C., & Karbing, D. (2022). Transparent decision support for mechanical ventilation using visualization of clinical preferences. *BioMedical Engineering OnLine*, *21*(1), 5.

Reinders, J., Hunnekens, B., van de Wouw, N., & Oomen, T. (2022). Noninvasive breathing effort estimation of mechanically ventilated patients using sparse optimization. *IEEE Open Journal of Control Systems*, *1*, 57–68.

Rietveld, T., van der Ster, B., Schoe, A., Endeman, H., Balakirev, A., Kozlova, D., Gommers, D., & Jonkman, A. (2025). Let's get in sync: current standing and future of AI-based detection of patient-ventilator asynchrony. *Intensive Care Medicine Experimental*, *13*(1), 39.

Rossi, A., Gottfried, S., Higgs, B., Zocchi, L., Grassino, A., & Milic-Emili, J. (1985). Respiratory mechanics in mechanically ventilated patients with respiratory failure. *Journal of Applied Physiology*, *58*(6), 1849–1858.

Sun, Q., Chase, J. G., Zhou, C., Tawhai, M., Knopp, J., Möller, K., Shaw, G., & Desaive, T. (2024). Estimating patient spontaneous breathing effort in mechanical ventilation using a b-splines function approach. *IFAC Journal of Systems and Control*, *28*, Article 100259.

Vicario, F., Albanese, A., Karamolegkos, N., Wang, D., Seiver, A., & Chbat, N. (2015). Noninvasive estimation of respiratory mechanics in spontaneously breathing ventilated patients: a constrained optimization approach. *IEEE Transactions on Biomedical Engineering*, *63*(4), 775–787.

Yoshida, T., & Brochard, L. (2018). Esophageal pressure monitoring: why, when and how? *Current Opinion in Critical Care*, *24*(3), 216–222.

Younes, M., Brochard, L., Grasso, S., Kun, J., Mancebo, J., Ranieri, M., Richard, J.-C., & Younes, H. (2007). A method for monitoring and improving patient: ventilator interaction. *Intensive Care Medicine*, *33*(8), 1337–1346.

Younes, M., Webster, K., Kun, J., Roberts, D., & Masiowski, B. (2001). A method for measuring passive elastance during proportional assist ventilation. *American Journal of Respiratory and Critical Care Medicine*, *164*(1), 50–60.

Zhang, B., Ratano, D., Brochard, L., Georgopoulos, D., Duffin, J., Long, M., Schepens, T., Telias, I., Slutsky, A., Goligher, E., et al. (2021). A physiology-based mathematical model for the selection of appropriate ventilator controls for lung and diaphragm protection. *Journal of Clinical Monitoring and Computing*, *35*, 363–378.